Check for updates

Achieving vibrational energies of diatomic systems with high quality by machine learning improved DFT method

Zhangzhang Yang, [ID] [a] Zhitao Wan,[a] Li Liu,[a] Jia Fu,*[a] Qunchao Fan,*[a] Feng Xie,[b] Yi Zhang[c] and Jie Ma[d]

When using *ab initio* methods to obtain high-quality quantum behavior of molecules, it often involves a lot of trial-and-error work in algorithm design and parameter selection, which requires enormous time and computational resource costs. In the study of vibrational energies of diatomic molecules, we found that starting from a low-precision DFT model and then correcting the errors using the high-dimensional function modeling capabilities of machine learning, one can considerably reduce the computational burden and improve the prediction accuracy. Data-driven machine learning is able to capture subtle physical information that is missing from DFT approaches. The results of $^{12}C^{16}O$, ^{24}MgO and $Na^{35}Cl$ show that, compared with CCSD(T)/cc-pV5Z calculation, this work improves the prediction accuracy by more than one order of magnitude, and reduces the computation cost by more than one order of magnitude.

1 Introduction

Diatomic molecules and their corresponding energy spectra are widely used in astrophysics, ultracold molecules, fundamental physical constants and thus on.[1–5] Various experimental techniques have been developed for high-precision spectra measurement such as velocity modulation laser spectroscopy (VMS),[6] noise immune cavity enhanced optical heterodyne molecular spectroscopy (NICE-OHMS),[7] laser-induced breakdown spectroscopy (LIBS)[8] and so forth. However, limited by experimental conditions, generally only part of the energy levels corresponding to lower quantum numbers can be measured accurately. In the theoretical side, there are two main options: (1) *ab initio* methods based on the principles of quantum mechanics, such as Hartree Fock and its extension, DFT, *etc.*[9–13] The post-Hartree Fock methods like multireference configuration interaction methods have decent performance in accuracy, whereas the steep computation cost and lengthy time make them limited to small systems.[12,14,15] The DFT

method is compromised in accuracy, but it has rapid calculation speed, which makes it the first choice for the calculation of large systems.[16–18] In order to improve the performance of DFT, both general and accurate exchange-correlation functionals and basis set are required,[16,18–20] which is still a challenge to us.[18,21,22] (2) Data driven algorithms, such as empirical potential energy function and direct parameter formulas for energy levels.[23,24] The accuracy of data driven algorithms are higher than *ab initio* methods except that they are only applicable to some molecular systems which have superior-quality experimental data.

Recently, the machine learning algorithm has made many achievements in spectroscopy study.[25–27] In this work, machine learning algorithm was applied to improve the performance of DFT in the study of diatomic vibrational spectrum. To obtain the best prediction, three widely used machine learning regression algorithms were tested with $H^{35}Cl$ as an example. Then, the best performing algorithm was used to predict the vibrational energy levels of $^{12}C^{16}O$, ^{24}MgO, and $Na^{35}Cl$. Finally, the spectral quality of many systems (^{24}MgO, HF, N_2, $H^{35}Cl$, $Na^{35}Cl$, $^{12}C^{16}O$, BeH, and SiN *et al.*) were greatly improved.

2 Theory and method

2.1 DFT for vibrational energies

For the purpose of obtain the vibrational energy spectrum of diatomic molecules systems, it is inevitable to solve the Schrodinger equation (r and R denote the electronic and the nuclear coordinate, respectively),

$$\hat{H}\Psi(r, R) = E\Psi(r, R), \tag{1}$$

[a]School of science, Key Laboratory of High Performance Scientific Computation, Xihua University, Chengdu, 610039, China. E-mail: zero15957168281@163.com; fujiayouxiang@126.com; fanqunchao@sina.com

[b]Institute of Nuclear and New Energy Technology, Collaborative Innovation Center of Advanced Nuclear Energy Technology, Key Laboratory of Advanced Reactor Engineering and Safety of Ministry of Education, Tsinghua University, Beijing, 100084, China

[c]College of Advanced Interdisciplinary Studies, National University of Defense Technology, Changsha, 410073, China

[d]State Key Laboratory of Quantum Optics and Quantum Optics Devices, Laser Spectroscopy Laboratory, College of Physics and Electronics Engineering, Shanxi University, Taiyuan, 030006, China

where $\hat{H}$, E and $\Psi(r, R)$ represent the Hamiltonian of the system, total energy and wave function, respectively. It is worth noting that the wave function must be first order continuous differentiable, square integrable, and so on, which makes the partial solutions of the Schrodinger equation called mathematical but nonphysical.[28] In other words, the wave function is the result of approximation. Then, when studying the radial motion of the binuclear system, taking nonrelativistic approximation and Born–Oppenheimer approximation (BOA) into consider, eqn (1) can be simplified to

$$\left\{ -\frac{\hbar^2 d^2}{2\mu dr^2} + V(r) + \frac{[J(J+1)]\hbar^2}{2\mu r^2} \right\} \varphi(r) = E_{vJ}\varphi(r). \quad (2)$$

where $\hbar = h/2\pi$ (h is the Planck constant), μ is the reduced mass of two nucleus, J is total angular momentum quantum number, r is internuclear distance, and $V(r)$ corresponds to the electrostatic interaction of all the particles.[23] One problem is that the exchange–correlation energy has no universal accurate form,[29] which introduces error to results. Finally, the ro-vibrational energy level E_{vJ} can be expressed as

$$E_{vJ} = G(v) + F_v(J), \quad (3)$$

and

$$G(v) = \omega_e \left(v + \frac{1}{2}\right) - \omega_e x_e \left(v + \frac{1}{2}\right)^2 + \omega_e y_e \left(v + \frac{1}{2}\right)^3 + \cdots, \quad (4)$$

$$F_v(J) = B_v \left[J\left(J + \frac{1}{2}\right)\right] - D_v \left[J\left(J + \frac{1}{2}\right)\right]^2 + H_v \left[J\left(J + \frac{1}{2}\right)\right]^3 + \cdots. \quad (5)$$

While $J = 0$, E_{vJ} degenerates to G_v, namely vibrational energy level.[30]

A conclusion is drawn that obtaining the vibrational energy levels of molecules, a large quantity of approximations need to be included, and various approximations affect each other. Error is often unavoidable and difficult to predict in advance.

2.2 Combining machine learning algorithm and DFT

2.2.1 Machine learning algorithm. Among a variety of machine learning (ML) regression algorithms, artificial neural network (ANN),[31,32] random forest (RF)[33,34] and extreme gradient boosting (XGBoost)[35] algorithms were widely used and usually found successful. All three algorithms have been tested in this work for vibrational energy prediction. The results were compared in the Fig. 1. The absolute error is the predicted values minus the experimental values. Clearly, ANN performs the best. Thus, it is the algorithm used in this work.

An ANN consists of an input layer of neurons, followed by many hidden layers (two, three or more layers are all fine), and a final layer of output neurons. Neurons are connected by weights V_{ij}. Given the input, x_j, the output, h_i, of neuron i is,

$$h_i = \sigma\left(\sum_{j=1}^{N} V_{ij}x_j + T_i^{hid}\right), \quad (6)$$

where $\sigma(*)$ is called activation function, N is the number of input neurons, and T_i^{hid} is the threshold term of the neurons.[31] It is worth noting that activation function not only introduces nonlinearity into the neural network, but also constrains the value of neurons to prevent the ANN from being paralyzed by divergent neurons. And a common example of the activation function is the sigmoid function,[31] defined as
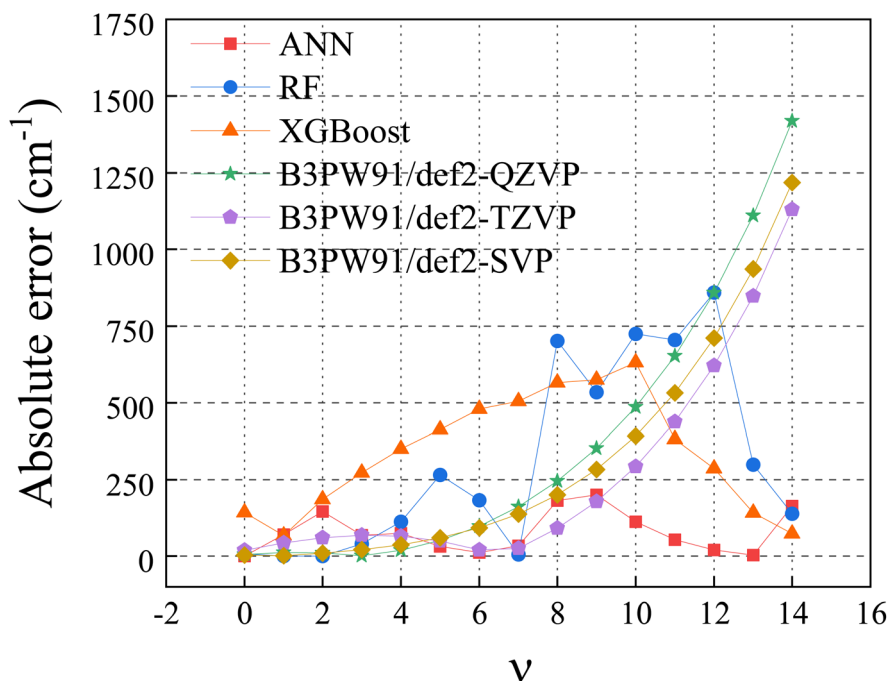
$$\sigma(u) = \frac{1}{1 + e^{-u}}. \quad (7)$$

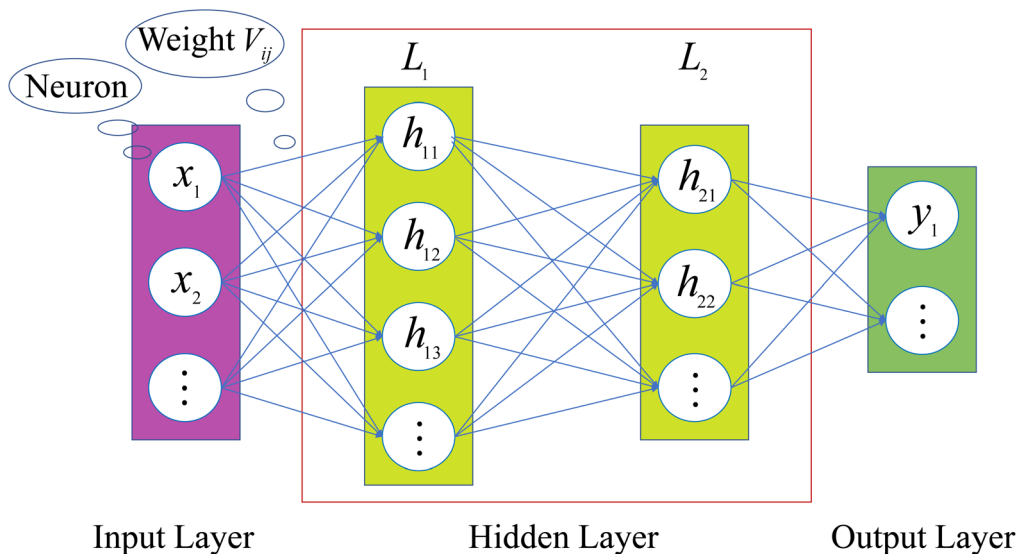Fig. 1 Absolute error of H^{35}Cl in ML algorithms and DFT methods.

Fig. 2 Architecture of an ANN.

The architecture is shown in Fig. 2. When ANN is used to establish a high-dimensional functional relationship between input and output variables, the data samples will be divided into three groups, namely training set, validation set, and test set. For convenience, the training set and the validation set are also called sub-sample set uniformly. Similar to how humans learn through feedback, neural networks obtain training errors through their performance on the training set. Then, the weights between the connected neurons are adjusted for

learning, which reduces the training error. The performance of ANN on the validation set is tracked during the learning process. And the one that performs the best is selected as the chosen model. Finally, the test set is used to determine the performance level of the ANN.[31]

2.2.2 Prediction of vibrational energies. By analyzing the error data between DFT and experimental results, a definite and clear trend is found. It is illustrated in Fig. 3 (take B3PW91/def2-QZVP as an example) that higher vibrational
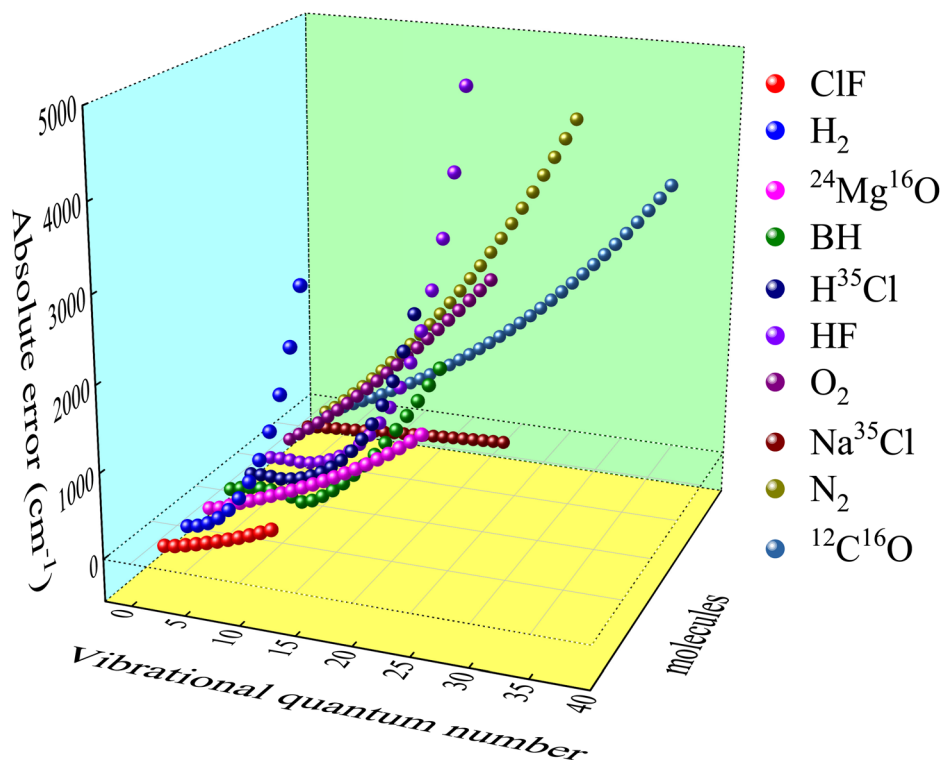

Fig. 3 Systematic error of B3PW91/def2-QZVP in vibrational energy levels prediction.

quantum number means greater error, and the error trajectories of different molecules are similar. The absolute error here is the theoretical vibrational energy minus the experiment value. This trend law with abundant details can be learned by ML method. Therefore, after getting the theoretical value E_v^{ab} of the DFT methods and the corresponding experimental results, the systematic error E_v^{sys} of DFT methods can be obtained through ANN. Ultimately, the predicted vibrational energy E_v is defined as

$$E_v(\alpha) = E_v^{ab} + E_v^{sys}(\alpha), \qquad (8)$$

where α represents the kind of diatomic molecular system. It's worth noting that $E_v^{sys}(\alpha)$ is an error function associated with molecules. So that it is not a fixed constant.

3 Results and discussion

3.1 Obtain initial sample set

The potential energy curves of 39 molecules, such as H_2, $^{12}C^{16}O$, ClF, *et al.*, were obtained by Gaussian 09 (ref. 36) with B3PW91/

Table 2 The input characteristic variables of ^{24}MgO (cm^{-1})

E_v^{QZ}	E_v^{TZ}	E_v^{S}
380.703	385.124	379.880
1203.812	1145.498	1141.218
2016.469	1894.550	1890.964
2818.615	2632.317	2629.060
3610.286	3358.877	3355.515
4391.528	4074.295	4070.334
5162.374	4778.626	4773.501
5922.839	5471.926	5465.001
6672.946	6154.270	6144.839
7412.729	6825.742	6813.034
8142.228	7486.417	7469.602
8861.481	8136.358	8114.558
9570.527	8775.622	8747.914
10 269.395	9404.272	9369.688
10 958.118	10 022.374	9979.911
11 636.728	10 630.005	10 578.627
12 305.264	11 227.241	11 165.886
12 963.767	11 814.158	11 741.743
13 612.285	12 390.825	12 306.256
14 250.864	12 957.311	12 859.483
14 879.549	13 513.684	13 401.489

Table 1 Partial experimental vibrational energy levels of molecules in the ground state (cm^{-1})

ν	BH	$^{12}C^{16}O$	$^{12}C^{17}O$	$^{12}C^{18}O$	$^{13}C^{16}O$	$^{13}C^{17}O$	$^{13}C^{18}O$	$^{14}C^{16}O$
0	1171.08	1081.77	1068.03	1055.71	1057.72	1043.66	1031.05	1036.74
1	3440.30	3225.04	3184.32	3147.84	3153.79	3112.11	3074.74	3091.61
2	5614.11	5341.83	5274.81	5214.74	5224.54	5155.92	5094.38	5122.15
3	7694.67	7432.21	7339.54	7256.48	7270.04	7175.14	7090.03	7128.44
4	9684.16	9496.24	9378.60	9273.14	9290.35	9169.83	9061.73	9110.52

ν	$^{14}C^{17}O$	$^{14}C^{18}O$	$^{24}Mg^{16}O$	$^{25}Mg^{16}O$	$^{26}Mg^{16}O$	SO	AlO	BeH
0	1022.39	1009.51	391.14	388.01	385.10	576.94	488.00	1021.30
1	3049.05	3010.88	1165.88	1156.60	1147.99	1740.42	1453.40	3008.15
2	5052.07	4989.20	1930.32	1915.05	1900.90	2916.75	2404.76	4921.11
3	7031.50	6944.51	2684.16	2663.08	2643.55	4105.98	3342.12	6760.67
4	8987.38	8876.87	3427.11	3400.42	3375.67	5308.16	4265.42	8527.35

ν	BeD	BeT	BF	ClF	$H^{35}Cl$	$H^{37}Cl$	$D^{35}Cl$	$D^{37}Cl$
0	759.86	649.25	742.00	390.50	1483.88	1482.76	1066.60	1065.04
1	2248.84	1925.35	2208.00	1164.00	4369.86	4366.64	3157.66	3153.10
2	3697.03	3171.70	3651.00	1927.60	7151.86	7146.69	5195.04	5187.63
3	5104.62	4388.42	5072.00	2681.20	9830.66	9823.69	7179.05	7168.96
4	6471.83	5575.64	6470.00	3424.50	12 406.70	12 398.10	9109.98	9097.36

ν	HF	DF	H_2	HBr	MgH	N_2	$Na^{35}Cl$	$Na^{37}Cl$
0	2050.77	1490.30	2170.88	1314.65	739.11	1175.77	181.90	179.94
1	6012.19	4396.97	6332.02	3873.57	2171.09	3505.69	543.05	537.24
2	9801.57	7212.12	10 257.99	6341.99	3539.79	5806.93	900.70	891.11
3	13 423.60	9937.66	13 953.23	8719.91	4841.14	8079.47	1254.89	1241.59
4	16 882.40	12 575.30	17 421.24	11 007.00	6070.50	10 323.30	1605.65	1588.71

ν	NaLi	O_2	SiC	SiCl	SiN	SiO
0	127.81	787.14	475.47	267.25	574.0616	619.20
1	384.08	2343.47	1416.67	798.54	1712.46	1848.90
2	631.07	3876.15	2344.87	1325.50	2837.85	3066.50
3	877.74	5385.51	3260.07	1847.50	3950.20	4272.30
4	1121.07	6871.86	4162.27	2365.50	5049.46	5466.10

Table 3 Main parameter settings of ANN[a]

Hidden layer 1	Hidden layer 2	trainRatio	valRatio	Train function	Error function	Divide function
30	20	0.85	0.15	trainbr	mse	Dividerand

[a] trainRatio = the number of train set/the number of subsample set. valRatio = the number of validation set/the number of subsample set.

def2-XVP (where X = QZ, TZ or S). Then E_v^{ab} was obtained by solving eqn (2) by LEVEL.[37] The corresponding data of partial experimental vibration energy levels[38–59] are displayed in Table 1 as the initial sample set. Finally, the predicted vibrational energy and relative deviation δ of the molecules are obtained through ANN. And the expression of δ is:

$$\delta = \left| \frac{E_v^* - E_v}{E_v} \right| \times 100\%, \qquad (9)$$

where E_v^* represents the theoretical energy (the value of DFT or ANN), E_v represents the experimental value. The input characteristic variables are shown below:

(1) Vibrational energy of B3PW91/def2-QZVP: E_v^{QZ};

(2) Vibrational energy of B3PW91/def2-TZVP: E_v^{TZ};

(3) Vibrational energy of B3PW91/def2-SVP: E_v^{S}.

The output variable is written as E_v^B. A case in point is ^{24}MgO in Table 2. The task of the ANN is to learn the correct mapping relationship between input characteristic variables and system deviation E_v^{sys}.

Table 4 Prediction of vibrational energies of $^{12}C^{16}O$/^{24}MgO/$Na^{35}Cl$ (cm^{-1})[a]

	$^{12}C^{16}O$			^{24}MgO			$Na^{35}Cl$		
ν	E_v	$E_v^B - E_v$	$E_v^5 - E_v$	E_v	$E_v^B - E_v$	$E_v^5 - E_v$	E_v	$E_v^B - E_v$	$E_v^5 - E_v$
0	1081.77	20.430	−41.597	391.14	−7.408	−24.315	181.90	−8.463	−5.210
1	3225.04	40.073	−47.228	1165.88	23.542	−67.207	543.05	−8.877	−13.490
2	5341.83	50.975	−52.550	1930.32	37.748	−105.760	900.70	−9.328	−21.736
3	7432.21	16.260	−57.526	2684.16	39.576	−139.913	1254.89	−9.697	−29.886
4	9496.24	−48.621	−62.174	3427.11	34.611	−169.528	1605.650	−9.806	−37.961
5	11 533.99	−21.454	−66.434	4158.89	28.412	−194.442	1953.01	−9.425	−45.949
6	13 545.54	66.471	−70.264	4879.21	24.892	−214.454	2297.02	−8.353	−53.853
7	15 530.95	21.302	−73.663	5587.77	24.813	−229.336	2637.69	−6.375	−61.666
8	17 490.31	29.300	−76.624	6284.28	25.498	−238.849	2975.08	−3.382	−69.383
9	19 423.68	18.285	−79.126	6968.45	22.793	−242.728	3309.20	0.641	−77.004
10	21 331.14	−32.063	−81.149	7640.00	15.022	−240.705	3640.09	5.541	−84.527
11	23 212.78	−44.368	−82.679	8298.63	5.976	−232.502	3967.80	10.937	−91.957
12	25 068.67	−13.295	−83.713	8944.06	2.979	−217.836	4292.33	16.183	−99.282
13	26 898.89	−44.542	−84.264	9575.98	9.678	−196.420	4613.74	20.281	−106.509
14	28 703.54	−10.990	−84.316	10 194.12	20.080	−167.961	4932.05	21.831	−113.634
15	30 482.68	12.240	−83.849	10 798.17	22.109	−132.166	5247.30	19.027	−120.651
16	32 236.41	4.691	−82.890	11 387.86	10.540	−88.739	5559.51	9.710	−127.571
17	33 964.80	1.2907	−81.508	11 962.89	−3.230	−37.381	5868.71	−8.600	−134.390
18	35 667.96	5.946	−79.757	12 522.96	−1.051	22.204	6174.94	−38.528	−141.106
19	37 345.95	−1.119	−77.713	13 067.80	8.500	90.311			
20	38 998.86	7.838	−75.525	13 597.10	−47.268	167.237			
21	40 626.79	3.069	−73.411						
22	42 229.80	0.363	−71.673						
23	43 807.99	−1.943	−70.756						
24	45 361.43	−0.141	−71.309						
25	46 890.20	−0.872	−74.258						
26	48 394.02	−2.294	−80.588						
27	49 874.02	−0.886	−93.253						
28	51 329.22	3.742	−113.948						
29	52 760.00	5.960	−146.852						
30	54 166.50	1.847	−196.933						
31	55 548.70	−1.806	−268.367						
32	56 906.67	−0.006	−360.419						
33	58 240.46	−0.339	−466.403						
34	59 550.10	−0.563	−583.000						

[a] E_v represents the experimental vibrational energy. E_v^B represents the vibrational energy predicted by machine learning method. E_v^5 represents the vibrational energy of CCSD(T)/cc-pV5Z.

3.2 Prediction results of vibrational energies

The initial sample set (39 molecules in all) was assigned to the sub-sample set (36 molecules) and the test set (3 molecules). After plenty of parameter set tests, and considering the calculation time and accuracy comprehensively, the most balanced set of parameters was chosen as the training parameters, which are listed in Table 3. The relative deviation (see eqn (9)) is used to measure the performance of ANN. For the test set consists of $Na^{35}Cl$, ^{24}MgO and $^{12}C^{16}O$, the average relative deviation of the final ANN model is 0.42%, the maximum relative deviation is 4.65%, the minimum relative deviation is 0.0000099%. On the sub-sample set, the average relative deviation is 1.10%, the maximum relative deviation is 15.92%, the minimum relative deviation is 0.0000038%. The result shows consistent performance on the training and sub-sample set, which means that the learned model is reliable.

3.3 Comparison and analysis

The comparison with CCSD(T)/cc-pV5Z results are listed in Table 4. As shown in Tables 2 and 4, it can be found that ANN can effectively improve the performance of B3PW91/def2-XVP,

even better than the more complex *ab initio* method (CCSD(T)/cc-pV5Z). In detail, the error of ab initial methods increases significantly at high energy levels and easily exceeds $100 \, cm^{-1}$, not to mention the maximum error of B3PW91/def2-QZVP exceeds $1000 \, cm^{-1}$. However, the maximum error of ANN does not exceed $70 \, cm^{-1}$, and the minimum error is only $0.006 \, cm^{-1}$. In addition, the error of the current method is smaller than that of CCSD(T) at each vibrational energy level.

In order to further illustrate the reliability of the current method, many more diatomic molecules have been studied and compared with CCSD(T)/cc-pV5Z. Some are shown in Fig. 4, the height of red pillar is the average relative deviation of CCSD(T)/cc-pV5Z and the height of blue pilar is the average relative deviation of ANN. It shows that the improvement in prediction introduced by ANN over the *ab initio* method is better than that obtained by expanding the basis set.

It should also be emphasized that this work also considerably reduces the computational cost. Taking $Na^{35}Cl$ for an example, it takes more than 40 hours to obtain the results of CCSD(T)/cc-pV5Z, compared to less than one hour for the current method, which includes preparing DFT data and executing the ANN algorithm.
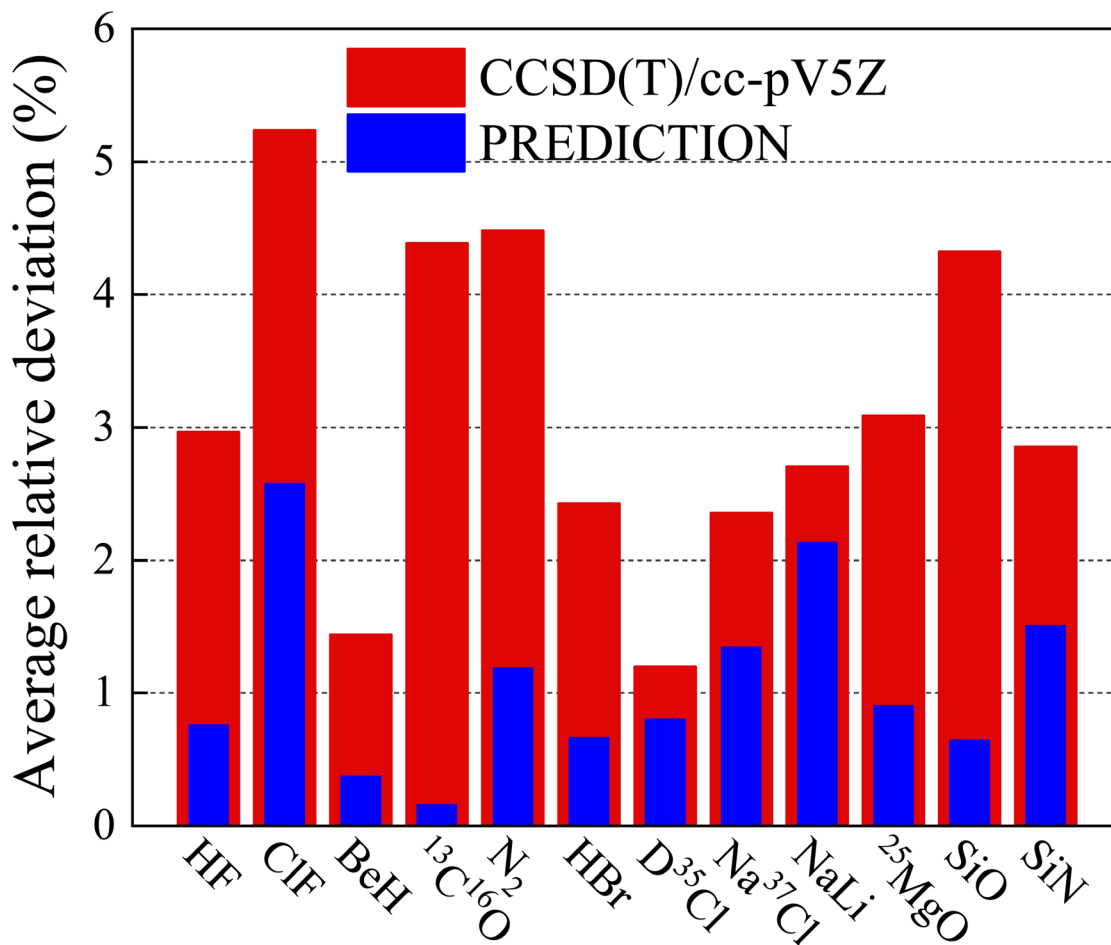

Fig. 4 Comparison of the average relative deviation of vibrational energy levels between ANN and CCSD(T)/cc-pV5Z.

4 Conclusion

In this work, a general method is presented to obtain vibrational spectra of diatomic molecules of high quality by starting from conventional DFT calculations and modifying them with artificial neural network models. This approach provides a different path to improve DFT results without introducing sophisticated models (such as specific hybrid functionals) and large basis sets. Compared with the results of CCSD(T)/cc-pV5Z, the current work reduces the vibrational energies prediction error for diatomic systems from hundreds to dozens, even to tenths, and takes less than a tenth of the time. Since the strategy employed in this paper is a general data-driven approach, it can be easily extended to calculations of other molecular properties. For example, current DFT calculations of fluorescence spectra of macromolecular systems can be easily exceed 1000 cm^{-1}.[60,61] In future work, it is expected that the fluorescence spectral prediction capability of DFT can be improved by building a fluorescence spectral data set and adopting a correction method similar to that used in this work. There are several keys that should be attention: (1) collect accurate experimental (or computational) data of macromolecular system properties to establish a data set; (2) from simple to complex, try a variety of DFT methods for these properties, so that the calculation error on the data set can show a certain trend (similar to Fig. 3); (3) build a high-dimensional function through ANN and learn the rule of calculation error; (4) combine DFT and ANN error model to achieve higher prediction quality.

Conflicts of interest

There are no conflicts to declare

Acknowledgements

Notes and references

1 M. S. Safronova, D. Budker, D. DeMille, D. F. J. Kimball, A. Derevianko and C. W. Clark, Search for new physics with atoms and molecules, *Rev. Mod. Phys.*, 2018, **90**, 025008.

2 C. R. Baiz, B. Błasiak, J. Bredenbeck, M. Cho, J.-H. Choi, S. A. Corcelli, A. G. Dijkstra, C.-J. Feng, S. Garrett-Roe, N.-H. Ge, M. W. D. Hanson-Heine, J. D. Hirst, T. L. C. Jansen, K. Kwac, K. J. Kubarych, C. H. Londergan, H. Maekawa, M. Reppert, S. Saito, S. Roy, J. L. Skinner, G. Stock, J. E. Straub, M. C. Thielges, K. Tominaga, A. Tokmakoff, H. Torii, L. Wang, L. J. Webb and M. T. Zanni, Vibrational Spectroscopic Map, Vibrational Spectroscopy, and Intermolecular Interaction, *Chem. Rev.*, 2020, **120**, 7152–7218.

3 D. J. Fink and E. G. Myers, Deuteron-to-proton mass ratio from simultaneous measurement of the cyclotron frequencies of H_2^+ and D+, *Phys. Rev. Lett.*, 2021, **127**, 243001.

4 Y. Li, T. Sato and K. L. Ishikawa, Implementation of a time-dependent multiconfiguration self-consistent-field method for coupled electron-nuclear dynamics in diatomic molecules driven by intense laser pulses, *Phys. Rev. A*, 2021, **104**, 043104.

5 W. Liu, J. Wu, J. Ma, P. Li, V. B. Sovkov, L. Xiao and S. Jia, Observation and analysis of the hyperfine structure of near-dissociation levels of the NaCs $c^3\sum^+$ state below the dissociation limit $3S_{1/2}+6P_{3/2}$, *Phys. Rev. A*, 2016, **94**, 032518.

6 G. Chen, X. Yang, X. Ying, G. Liu, Y. Huang and Y. Chen, Optical heterodyne detected velocity modulation molecular ionic spectroscopy, *Chin. Sci. Bull.*, 2004, **49**, 2354–2359.

7 A. Foltynowicz, F. M. Schmidt, W. Ma and O. Axner, Noise-immune cavity-enhanced optical heterodyne molecular spectroscopy: current status and future potential, *Appl. Phys. B: Photophys. Laser Chem.*, 2008, **92**, 313–326.

8 F. J. Fortes, J. Moros, P. Lucena, L. M. Cabalín and J. J. Laserna, Laser-induced breakdown spectroscopy, *Anal. Chem.*, 2013, **85**, 640–669.

9 A. Kolezynski and M. Krol, *Molecular Spectroscopy—Experiment and Theory: From Molecules to Functional Materials*, Springer International Publishing, Berlin, 2019, pp. 1–48.

10 H. Lischka, D. Nachtigallová, A. J. A. Aquino, P. G. Szalay, F. Plasser, F. B. C. Machado and M. Barbatti, Multireference approaches for excited states of molecules, *Chem. Rev.*, 2018, **118**, 7293–7361.

11 S. Bubin, M. Pavanello, W. C. Tung, K. L. Sharkey and L. Adamowicz, Born–Oppenheimer and Non-Born–Oppenheimer, atomic and molecular calculations with explicitly correlated Gaussians, *Chem. Rev.*, 2013, **113**, 36–79.

12 M. Chen and D. A. Dixon, Low-Lying electronic states of irn clusters with n = 2–8 predicted at the DFT, CASSCF, and CCSD(T) levels, *J. Phys. Chem.*, 2013, **117**, 3676–3688.

13 R. Liu, R. Wang, D. Li, Y. Zhu and X. Yang, An *ab initio* study on boundaries for characterizing cooperative effect of hydrogen bonds by intermolecular compression, *Chin. Chem. Lett.*, 2022, 107857.

14 T. Jonathan, L. Lorenzo, K. M. Laura and N. Y. Sergei, The *ab initio* calculation of spectra of open shell diatomic molecules, *J. Phys. B: At. Mol. Opt. Phys.*, 2016, **40**, 102001.

15 J. Fu, J. Jian, S. Long, Z. Fan, Q. Fan, F. Xie, Y. Zhang and J. Ma, Study on potential energy curves and ro-vibrational energies of DT, HT and T2 molecules, *Spectrochim. Acta, Part A*, 2021, **260**, 119913.

16 M. A. Palafox, DFT computations on vibrational spectra: scaling procedures to improve the wavenumbers, *Phys. Sic. Rev.*, 2018, **3**, 20170184.

17 A. Erba, J. Baima, I. Bush, R. Orlando and R. Dovesi, Large-Scale condensed matter DFT simulations: performance and capabilities of the CRYSTAL Code, *J. Chem. Theory Comput.*, 2017, **13**, 5019–5027.

18 S. Mohr, L. E. Ratcliff, L. Genovese, D. Caliste, P. Boulanger, S. Goedecker and T. Deutsch, Accurate and efficient linear scaling DFT calculations with universal applicability, *Phys. Chem. Chem. Phys.*, 2015, **17**, 31360–31370.

19 G. Rauhut, S. Puyear, K. Wolinski and P. Pulay, Comparison of NMR Shielding calculated from Hartree-Fock and density Functional wave functions using gauge-including atomic orbitals, *J. Phys. Chem.*, 1996, **100**, 6310–6316.

20 G. Rauhut and H. Werner, The vibrational spectra of furoxan and dichlorofuroxan: a comparative theoretical study using density functional theory and local electron correlation methods, *Phys. Chem. Chem. Phys.*, 2003, **5**, 2001–2008.

21 A. J. Cohen, P. Mori-Sanchez and W. Yang, Insights into current limitations of density functional theory, *Science*, 2008, **321**, 792–794.

22 Y. Zhang, X. Xu and W. A. Goddard III, Doubly hybrid density functional for accurate descriptions of nonbond interactions, thermochemistry, and thermochemical kinetics, *Proc. Natl. Acad. Sci. U. S. A.*, 2009, **106**, 4963–4968.

23 J. Fu, S. Long, J. Jian, Z. Fan, Q. Fan, F. Xie, Y. Zhang and J. Ma, A joint data and model driven method for study diatomic vibrational spectra including dissociation behavior, *Spectrochim. Acta, Part A*, 2020, **239**, 118363.

24 C. A. Onate, I. B. Okon, M. C. Onyeaju and O. Ebomwonyi, Vibrational energies of some diatomic molecules for a modified and deformed potential, *Sci. Rep.*, 2021, **11**, 22498.

25 J. Zhao, G. Tian, Y. Qiu and H. Qu, Rapid quantification of active pharmaceutical ingredient for sugar-free Yangwei granules in commercial production using FT-NIR spectroscopy based on machine learning techniques, *Spectrochim. Acta, Part A*, 2011, **245**, 118878.

26 H. Li, Z. Xiang, C. Qin, Y. Li and M. Sun, Spectra-based blood species discrimination by machine learning: between human and non-human, *Infrared Phys. Technol.*, 2022, **122**, 104062.

27 J. Niskanen, A. Viadyka, J. A. Kettunen and C. J. Sahle, Machine learning in interpretation of electronic core-level spectra, *J. Electron Spectrosc. Relat. Phenom.*, 2022, **260**, 147243.

28 L. Piela, *Ideas of Quantum Chemistry – Volume 1: From Quantum Physics to Chemistry*, Elsevier, Amsterdam, 3rd edn, 2020, p. 764.

29 L. Piela, *Ideas of Quantum Chemistry, vol. 2, Interactions*, Elsevier, Amsterdam, 3rd edn, 2020, p. 660.

30 B. P. Stoicheff, High resolution Raman spectroscopy of Gasesix. spectra of H_2, HD, and D_2, *Can. J. Phys.*, 1957, **35**, 730–741.

31 S. C. Wang, *Artificial Neural Network*, Springer, Boston, 2003, p. 743.

32 O. I. Abiodun, A. Jantan, A. E. Omolara, K. V. Dada, N. A. Mohamed and H. Arshad, State-of-the-art in artificial neural network applications: a survey, *Heliyon*, 2018, **4**, e00938.

33 Y. Li, C. Zou, M. Berecibar, E. Nanini-Maury, J. C. W. Chan, P. V. D. Bossche, J. V. Mierlo and N. Omar, Random forest regression for online capacity estimation of lithium-ion batteries, *Appl. Energy*, 2018, **232**, 197–210.

34 E. M. Abdel-Rahman, F. B. Ahmed and R. Ismail, Random forest regression and spectral band selection for estimating sugarcane leaf nitrogen concentration using EO-1 Hyperion hyperspectral data, *Int. J. Rem. Sens.*, 2013, **32**, 712–728.

35 T. Chen and C. Guestrin, *Proceedings of the 22nd ACM SIGKDD International Conference on Knowledge Discovery and Data Mining*, 2016, p. 785.

36 M. J. Frisch, G. W. Trucks, H. B. Schlegel and G. E. Scuseria, et al., *Gaussian 09, Revision A. 02*, Gaussian, Inc., Wallingford ct, 2016.

37 R. J. Le Roy, LEVEL: a computer program for solving the radial Schrödinger equation for bound and quasibound levels, *J. Quant. Spectrosc. Radiat. Transfer*, 2017, **186**, 167–178.

38 K. A. Peterson and R. C. Woods, An *ab initio* investigation of the spectroscopic properties of BCl, CS, CCl^+, BF, CO, CF^+, CN_-, and NO^+, *J. Chem. Phys.*, 1987, **87**, 4409–4418.

39 M. A. A. Clyne and I. S. McDermid,

$$B^3 \prod (O^+)$$

states of IF, ICl and IBr. Part 1 — Calculation of the RKR turning points and Franck–Condon factors for the B–X Systems, *J. Chem. Soc.*, 1976, **72**, 2242–2251.

40 J. A. Coxon and P. G. Hajigeorgiou, Born–Oppenheimer breakdown in the ground state of carbon monoxide: a direct reduction of spectroscopic line positions to analytical radial Hamiltonian operators, *Can. J. Phys.*, 1992, **70**, 40–54.

41 R. S. Ram, M. Dulick, B. Guo, K. Q. Zhang and P. F. Bernath, Fourier transform infrared emission spectroscopy of NaCl and KCl, *J. Mol. Spectrosc.*, 1997, **183**, 360–373.

42 M. D. Saksena, M. N. Deo, K. Sunanda, S. H. Behere and C. T. Londhe, Fourier transform spectral study of $B^2\sum^+ - X^2\sum^+$ system of AlO, *J. Mol. Spectrosc.*, 2008, **247**, 47–56.

43 A. Shayesteh, R. D. E. Henderson, R. J. Le Roy and P. F. Bernath, Ground State PotentialEnergy Curve and Dissociation Energy of MgH, *J. Phys. Chem. A*, 2007, **111**, 12495–12505.

44 J. A. Coxon and P. G. Hajigeorgiou, Isotopic dependence of Born-Oppenheimer breakdown effects in diatomic hydrides: the $B^1\sum^+$ and $X^1\sum^+$ states of HF and DF, *J. Mol. Spectrosc.*, 1990, **142**, 254–278.

45 J. A. Coxon and P. G. Hajigeorgiou, Improved direct potential fit analyses for the ground electronic states of the hydrogen halides: HF/DF/TF, HCl/DCl/TCl, HBr/DBr/TBr and HI/DI/TI, *J. Quant. Spectrosc. Radiat. Transfer*, 2015, **151**, 133–154.

46 C. E. Blom, H. G. Hedderich, F. J. Lovas, R. D. Suenram and A. G. Maki, Infrared and microwave spectra of SrO and BaO, *J. Mol. Spectrosc.*, 1992, **152**, 109–118.

47 S. Edwards, J. Y. Roncin, F. Launay and F. Rostas, The Electronic Ground State of Molecular Nitrogen, *J. Mol. Spectrosc.*, 1993, **162**, 257–267.

48 T. G. Slanger and P. C. Cosby, Oxygen spectroscopy below 5.1 eV, *J. Phys. Chem.*, 1988, **92**, 267–282.

49 R. J. Le Roy, D. R. T. Appadoo, R. Colin and P. F. Bernath, On the $X^2\sum^+$, $A^2\prod$, and $C^2\sum^+$ states of BeH, BeD, and BeT, *J. Mol. Spectrosc.*, 2006, **236**, 178–188.

50 R. R. Reddy, T. V. R. Rao and R. Viswanath, Potential energy curves and dissociation energies of NbO, SiC, CP, PH^+, SiF^+, and NH^+, Astrophys, *Space Sci.*, 1992, **189**, 29–38.

51 R. S. Speth, C. Braatz and E. Tiemann, REMPI spectroscopy of SO singlet states, *J. Mol. Spectrosc.*, 1998, **192**, 69–74.

52 R. R. Reddy, Y. N. Ahammed, K. R. Gopal, P. A. Azeem and S. Anjaneyulu, RKRV potential energy curves, dissociation energies, γ-Centroids and Franck-Condon factors Of YO, CrO, BN, ScO,SiO And AlO Molecules, *Astrophys. Space Sci.*, 1998, **262**, 223–240.

53 M. Venkataramanaiah and S. V. J. Lakshman, Potential energy curves and dissociation energy of SiCl, *J. Quant. Spectrosc. Radiat. Transfer*, 1981, **26**, 11–13.

54 Z. L. Cai, J. M. L. Martin, J. P. François and R. Gijbels, Ab initio study of the $X^2\sum^+$ and $A^2\prod$ states of the SiN radical, *Chem. Phys. Lett.*, 1996, **252**, 398–404.

55 P. Botschwina, Spectroscopic properties of BH, BF, and HBF^+ calculated by SCEP-CEPA, *J. Mol. Spectrosc.*, 1986, **118**, 76–87.

56 I. Dabrowski, The Lyman and Werner bands of H_2, *Can. J. Phys.*, 1984, **62**, 1639–1664.

57 C. E. Fellows, J. Vergs and C. Amiot, The NaLi electronic ground state studied by laser induced fluorescence and Fourier transform spectroscopy, *Mol. Phys.*, 1988, **63**, 1115–1122.

58 J. A. Coxon and P. G. Hajigeorgiou, The Radial Hamiltonians for the $X^1\sum^+$ and $B^1\sum^+$ states of HCl, *J. Mol. Spectrosc.*, 2000, **203**, 49–64.

59 R. R. Reddy, Y. N. Ahammed, D. B. Basha, K. Narasimhulu, L. S. S. Reddy and K. R. Gopal, Spectroscopic studies of atmospheric interest on NO and NO^+, *J. Quant. Spectrosc. Radiat. Transfer*, 2006, **97**, 344–453.

60 D. Jacquemin, E. A. Perpete, G. Scalmani, M. J. Frisch, H. Ciofini and C. Adamo, Fluorescence of 1,8-naphthalimide: a PCM-TD-DFT investigation, *Chem. Phys. Lett.*, 2007, **448**, 3–6.

61 Y. Cui, Y. Zhang, K. Xie and W. Dong, A Newly Synthesized Heterobimetallic $Ni^{II}−Gd^{III}$ Salamo-BDC-Based Coordination Polymer: Structural Characterization, DFT Calculation, Fluorescent and Antibacterial Properties, *Crystals*, 2019, **9**, 596.